Applied Physics Express

LETTERS • **OPEN ACCESS**

Optical control of magnetization dynamics in Gd–Fe–Co films with different compositions

OPEN ACCESS

Applied Physics Express **10**, 103002 (2017)

https://doi.org/**10.7567/APEX.10.103002**

Optical control of magnetization dynamics in Gd–Fe–Co films with different compositions

Takuo Ohkochi[1]*, Hidenori Fujiwara[2], Masato Kotsugi[1†], Hirokazu Takahashi[3], Roman Adam[4], Akira Sekiyama[2], Tetsuya Nakamura[1], Arata Tsukamoto[5], Claus M. Schneider[4], Hiroto Kuroda[6‡], Elvis F. Arguelles[7], Mamoru Sakaue[7], Hideaki Kasai[7,8], Masakiyo Tsunoda[3], Shigemasa Suga[4,9], and Toyohiko Kinoshita[1]

[1]*Japan Synchrotron Radiation Research Institute, Sayo, Hyogo 679-5198, Japan*
[2]*Graduate School of Engineering Science, Osaka University, Toyonaka, Osaka 560-8531, Japan*
[3]*Department of Electronic Engineering, Tohoku University, Sendai 980-8579, Japan*
[4]*Peter Grünberg Institut (PGI-6), Research Center Jülich, D-52425 Jülich, Germany*
[5]*College of Science and Technology, Nihon University, Funabashi, Chiba 274-8501, Japan*
[6]*Department of Ophthalmology and Advanced Laser Medical Center, Faculty of Medicine, Saitama Medical University, Moroyama, Saitama 350-0495, Japan*
[7]*Graduate School of Engineering, Osaka University, Suita, Osaka 565-0871, Japan*
[8]*National Institute of Technology, Akashi College, Akashi, Hyogo 674-8501, Japan*
[9]*Institute of Scientific and Industrial Research, Osaka University, Ibaraki, Osaka 567-0047, Japan*

*E-mail: o-taku@spring8.or.jp
†Present address: Faculty of Industrial Science and Technology, Tokyo University of Science, Katsushika, Tokyo 125-8585, Japan
‡Present address: Laboratory for Advanced Laser Medicine, Faculty of Medicine, Aichi Medical University, Tama, Tokyo 206-0014, Japan

Received June 21, 2017; accepted August 15, 2017; published online September 12, 2017

Perpendicularly magnetized ferrimagnetic Gd–Fe–Co thin films with different compositions and multilayer arrangements were subjected to femtosecond laser pulses. The pulses triggered different magnetization dynamics in the various thin films. In the $Gd_{26}Fe_{66}Co_8$ film, which has an angular-momentum-compensation temperature (T_A) well above ambient temperature (T_{exp}), monotonic magnetization reversal occurred, whereas the $Gd_{22}Fe_{70}Co_8$ film (where T_A is well below T_{exp}) exhibited remarkable wavelike spin modulation with spatial inhomogeneity during relaxation of the laser-induced nonequilibrium state. These findings can enable broad-range tuning of the magneto-optical responses of Gd–Fe–Co alloys, facilitating advances in materials engineering. © 2017 The Japan Society of Applied Physics

Ultrafast manipulation of magnetization in ferrimagnetic thin films by femtosecond laser pulses has been intensively studied, both experimentally and theoretically. The magnetization dynamics has gradually become understood, and other physical phenomena have been discovered in related studies, inspiring strong interest in nonequilibrium magnetism. Circularly polarized light elicits direction-selective magnetization rotation or switching in ferrimagnetic alloys,[1–6] which has attracted much attention for its scientific significance and application potential. Even linearly polarized light triggers clear magnetization reversal in 4f–3d ferrimagnetic alloys.[7,8]

However, the responses of materials to laser pulses are not limited to magnetization switching. The electric and magnetic field vectors of laser beams can interact strongly with electrons in materials, generating coherent magnons[9–12] and plasmons.[13] Laser-triggered superdiffusive spin currents have transiently modified the equilibrium spin populations in specially designed magnetic structures.[14,15] These examples show that ultrafast pulsed lasers can not only control the magnetic states in custom-designed materials and structures, but can also answer fundamental research questions.

In this paper, we expose Gd–Fe–Co ferrimagnetic films with different compositions and multilayer structures to femtosecond laser pulses and systematically study their magnetization responses. Figure 1 schematizes the temperature-dependent spin dynamics around the angular-momentum-compensation point in ferrimagnetic systems.[16] When the angular-momentum-compensation temperature T_A is below or above the experimental temperature T_{exp}, we expect prolonged magnetization precession or rapid magnetization switching,

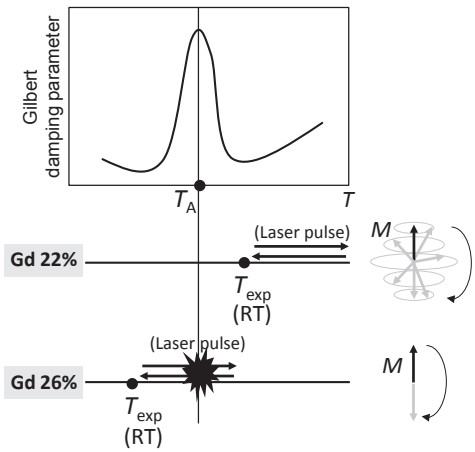

Fig. 1. Schematic of magnetization reversals induced by laser pulses. The angular momentum compensation temperature T_A is equivalent to a singular point of precession damping.[16] When the Gd content is 22% and $T_A < T_{exp}$ (RT), the sample temperature does not intercept T_A, and long-lasting magnetization precession is expected. When the Gd content is 26% and $T_A > T_{exp}$, smooth magnetization reversal with strong damping is expected.

respectively. In a Gd–Fe–Co film with a Gd content of 22% [$T_A < T_{exp}$ (room temperature, RT)], we observed anomalous wavelike modulation. In a detailed analysis, the wavelike magnetic modulation was explained well by intense resonant precession with weak damping, accompanied by a heat-induced lateral shift in the precession as an extrinsic perturbation.

Perpendicularly magnetized Gd–Fe–Co thin films were grown by magnetron sputtering. The designed multilayer structure was Ta (1 nm)/Ru (1 nm)/Gd–Fe–Co (20 nm)/

Ru (20 nm)/Ta (5 nm)/glass (substrate). For comparison, we tested $Gd_{22}Fe_{70}Co_8$ and $Gd_{26}Fe_{66}Co_8$ films with and without a 5-nm-thick Si_3N_4 heat-blocking layer grown between the $Gd_{26}Fe_{66}Co_8$ (20 nm) and Ru (20 nm) layers (hereafter, these three samples are referred to as Gd22%, Gd26%, and Gd26%–Si_3N_4, respectively). Time-resolved photoemission electron microscopy (PEEM) experiments were performed at the BL25SU soft X-ray beamline at SPring-8 using the X-ray magnetic circular dichroism (XMCD) effect at the Gd M_5 absorption edge. The experimental setup for the time-resolved XMCD-PEEM measurement is similar to that used in our previous study,[17] and a timing diagram of the pump–probe measurements is presented in Fig. S1 in the online supplementary data at http://stacks.iop.org/APEX/10/103002/mmedia. Linearly polarized laser pulses ($\lambda = 800$ nm, 120 fs, 5 kHz) were incident at 60° from the sample surface normal. The laser energy was set to ~4 μJ per pulse, and the radiation spot on the sample surface was elliptical with an approximate size of $125 \times 250\,\mu m^2$ (full width at half-maximum), which corresponds to a power density of ~16 mJ/cm^2. After each pump–probe cycle, the magnetization of the sample was initialized by a magnetic field pulse (XMCD-PEEM observations were performed under zero magnetic field). Static XMCD-PEEM imaging at room temperature confirmed that in the Gd26% and Gd22% samples, the Gd magnetization was aligned parallel and antiparallel to the direction of the applied magnetic field, respectively (data not shown). This indicates that the magnetization-compensation temperatures (T_M) were above and below RT in Gd26% and Gd22%, respectively (to compare the dynamics on the same gray-scale contrast, we applied the magnetic field pulse to the Gd26% and Gd22% samples in opposite directions). Apart from one comparative experiment [shown later in Fig. 4(b)], all the experiments were performed at RT.

Figure 2(a) shows a static XMCD-PEEM image of the initially homogeneously magnetized Gd26% sample after in situ excitation by a single ultrashort laser pulse with a fluence of ~16 mJ/cm^2. The magnetization was clearly reversed from the initial spin-down (black region) direction to the spin-up (white) direction in an elliptical area around the center of the excitation spot. Because the T_A value of this sample exceeds RT, the magnetization precession should be abruptly damped; that is, the local magnetization vector should quickly settle in the reversed direction.[16] Figure 2(b) shows the result for the Gd22% sample under the same excitation conditions. In this sample, there is no homogeneous magnetization reversal, but a fine-grained multidomain pattern formed, suggesting that most of the excitation energy was converted into intense spin precessions rather than magnetization reversal.

Figures 2(c) and 2(d) show time-dependent XMCD-PEEM images of the Gd26% and Gd22% samples, respectively. We define Δt as the delay time after laser irradiation. In the Gd26% sample [Fig. 2(c)], the magnetization generally settled to its final state approximately 1 ns after excitation. However, in the Gd22% sample [Fig. 2(d)], a packet of wavelike magnetization modulation propagated isotropically along the radial direction from 800 ps to 5 ns post-irradiation (Movie S2 in the online supplementary data at http://stacks.iop.org/APEX/10/103002/mmedia). Note that no sign of a wavelike feature appeared in the Gd26% sample.

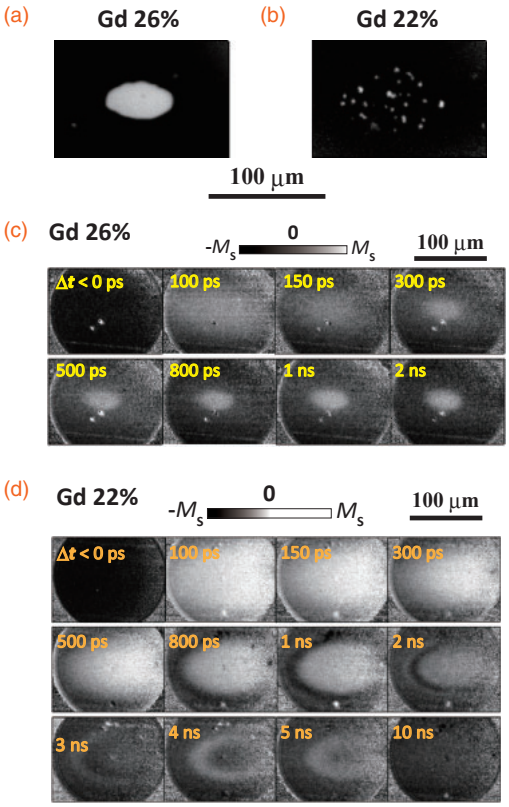

Fig. 2. Static XMCD-PEEM images at the Gd M_5 edge in the (a) Gd26% and (b) Gd22% samples at a long time after the laser pulse. Pump–probe XMCD-PEEM images at the Gd M_5 edge in the (c) Gd26% and (d) Gd22% samples at various times after an incident laser pulse.

Figure 3(a) traces the XMCD intensities of the Gd22% sample at $\Delta t = 1.5$ ns. The profile was traced along line AO [marked at the top and in the inset of Fig. 3(a)]. Also plotted are the net magnetization distribution (M_{net}) excluding the modulating component (blue dashed line) and the sinusoidal curve fitted to the data (red solid line). The fitting parameters [wavelengths (λ) and XMCD signal amplitudes ($|A_{XMCD}|$)] in regions I–III of Fig. 3(a) are summarized in Table I. The spatial variation in the parameters reflects the inhomogeneity in the laser-beam intensity profile. However, the XMCD modulation amplitudes ($|A_{XMCD}|$) are surprisingly large overall, ranging from 20 to 32% of M_{net}.

Figures 3(b) and 3(c) show complete profiles of the evolving space- and time-resolved magnetization and the wave shape simulated from this set of transient curves, respectively. In the calculated oscillation of the XMCD intensity, precessional spin motion was assumed. The XMCD signal was detected as a projected component of the magnetization parallel to the SR direction [see Fig. 3(d)]. For simplicity, we assumed that the precession frequency, wavelength, and angle of the waves were spatially and temporally uniform. The effects of the finite temporal resolution and the relevant sampling points are presented in Fig. S3 in the online supplementary data at http://stacks.iop.org/APEX/10/103002/mmedia. In Fig. 3(b), the wave frequency appears to be between 100 MHz and 1 GHz (period = 1–10 ns). However, considering an aliasing effect due to discrete and unevenly spaced sampling, a much higher frequency was needed to reproduce the features of the experimental profiles [sampling points are indicated by blue dots in Fig. 3(b)].

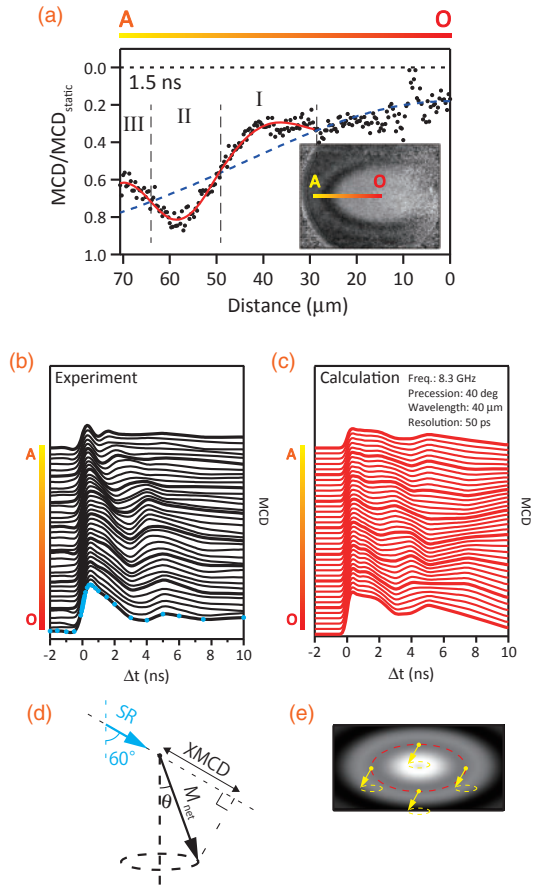

Fig. 3. (a) Line profile of XMCD intensities (black dots) of the Gd22% sample at post-irradiation time $\Delta t = 1.5$ ns. Inset shows an XMCD-PEEM image taken at this time. The profile is fitted to a sinusoidal function (red line) assuming a Gaussian distribution of the net magnetic moment (M_{net}, blue dashed line). The parameters are individually set in regions I–III. (b) Time evolution of the XMCD intensities at selected points along line AO. Blue dots in the bottommost plot show the delay times at which the XMCD-PEEM images were obtained. (c) Wave simulation results based on (b). (d) Relative configuration between the magnetization and synchrotron-radiation soft X-rays (SR). (e) Schematic of the relative magnetization directions along the circumferential direction, derived from the observed XMCD profiles.

Table I. Wavelength (λ) and XMCD modulation amplitude relative to M_{net} ($|A_{XMCD}|$), fitted to examine the sine wave component of the magnetization modulations in Fig. 3(a).

Region	λ (μm)	$\lvert A_{XMCD}\rvert$ (% of M_{net})
I	42.6	32.2
II	28.8	24.2
III	26.0	20.2

After varying the frequency parameter in the waveform simulations, we found that settings of 6.3, 8.3, 10.3,… GHz rather than of 100 MHz–1 GHz yielded strong agreement between the simulated and experimental waveforms [the waveform at an 8.5 GHz precession frequency is shown in Fig. 3(c)]. These frequencies are consistent with the ferromagnetic resonance (FMR) frequencies expected in ferrimagnetic systems.[16] The precession angle simply estimated from the modulation of the XMCD intensity was approximately 20° (±10°). However, when accounting for the finite temporal resolution of the experiment (50 ps), which reduced the amplitude of the 8.3 GHz waves, the precession angle approximately doubled [to ~40° (±20°)].

Note that the XMCD signals reflect both the out-of-plane and in-plane components of the magnetization [Fig. 3(d)]. Further, the XMCD-PEEM contrast exhibits a perfectly uniform concentric distribution. To match this observation, the precession phase of the magnetization should be identical along the circumferential direction [Fig. 3(e)]. In the absence of a magnetic field, the initial magnetization is directed perpendicular to the sample plane; hence, we infer that the incident direction of an obliquely incident laser pulse will determine the direction of the initial in-plane torque applied to the magnetization (the experimental geometry is detailed in Fig. S1 in the online supplementary data at http://stacks.iop.org/APEX/10/103002/mmedia). The wave front propagation in Fig. 2(d) is reminiscent of that of coherent magnons, but the nonzero momentum (*traveling* of the wave fronts) is likely produced by extrinsic factors such as lateral shifting of the precession phase induced by the radial heat gradient. External momentum sources are inferred from (i) the large wavelength (on the order of 10 μm), which exceeds that of magnons generated in metallic systems, (ii) the limitation of the observed modulation to the irradiated area, and (iii) the contraction and inward movement of the wave fronts toward the center of the spot (note that backward-volume magnetostatic waves[9]) are ruled out by the experimental geometry, which directs the magnetization perpendicular to the propagation direction of the waves). Considerations (ii) and (iii) strongly suggest that the wave fronts are driven by thermal and effective-field gradients created within the illuminated area. Shrinkage of the waving region suggests that the precession initially relaxes at the edge of the irradiated spot, where the system is promptly cooled. This picture is consistent with the results in Table I. The precession (characterized by $|A_{XMCD}|$ normalized by M_{net}) is less intense at the edge of the spot (region III) than in the central area (region I). The smaller wavelength in region III than in region I is attributed to the steep effective field created by adjacent magnetization standing perpendicular to the surface.

Although our simulation can consistently explain the wavelike modulations of the XMCD contrast by assuming (FMR-like) high-frequency magnetization precession, it does not uniquely determine the exact magnetization dynamics. To overcome this limitation, we further verified that the present magnetic modulation originates from the precessional motion (Fig. 1). Figure 4(a) shows the domain pattern of the Gd26%–Si_3N_4 sample excited in the same way as the Gd26% and Gd22% samples. The domain shape is complex and quite different from that of Gd26%, despite the identical composition of the two films. The pattern somewhat resembles that of the Gd22% sample [Fig. 2(b)] but develops no wavelike feature during the post-excitation sequence of nonequilibrium states [see Fig. 4(c)]. These peculiar results imply that the domain structures in Gd22% and Gd26%–Si_3N_4 are created by completely different mechanisms. In the Gd26%–Si_3N_4 sample, laser-induced heat diffuses very slowly through the Si_3N_4 heat-blocking layer, forming random domains. On the other hand, the Gd22% sample [Fig. 2(b)] possesses a fine domain structure originating from significant spin precession (as explained in Fig. 1). Figure 4(b) shows the domain structure of the Gd22% sample at a temperature much lower

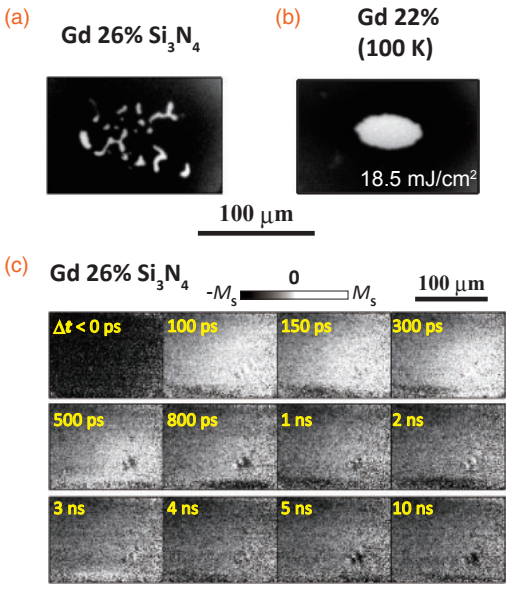

Fig. 4. Static XMCD-PEEM images at the Gd M_5 edge in the (a) Gd26%–Si_3N_4 sample taken at RT and (b) Gd22% sample taken at 100 K. For Gd22%, owing to the lower sample temperature, excitation requires a slightly larger fluence (18.5 mJ/cm^2) than that at RT (16 mJ/cm^2). (c) Pump–probe XMCD-PEEM images at the Gd M_5 edge in the Gd26%–Si_3N_4 sample.

than the sample's T_A (namely, at 100 K). The film shows clear magnetic reversal, analogous to that observed in the Gd26% sample. This proves that the properties of the magnetization dynamics are determined by T_A relative to T_{exp}.[16] From these results and discussions, we conclude that the resonant precession inherent in low-T_A systems is essential to generating anomalous spin dynamics, such as those shown in Fig. 2(d).

In conclusion, the magnetic domain structures and spin dynamics of the Gd–Fe–Co layer in multilayer thin films can be controlled by changing the alloy composition of the Gd–Fe–Co layers or the multilayer structure of the film. Comparing our results with those of Ref. 18, which reported monotonic magnetization reversal even in Gd22% samples, we confirmed that the magnetization response of the sample depends not only on the T_A value of its Gd–Fe–Co layer, but also on its multilayer structure. Although the *quasi-spin-waves* observed in our experiments may not qualify as coherent magnons,[9–12] we achieved an unprecedentedly large precession angle of the induced waves (on the order of 10°). Considering that low-frequency precession is allowed within the uncertainty of our present experiment, and knowing that anomalous behavior occurs in samples with specific heat conduction, experimental and theoretical searches for spin–phonon coupling[19,20] may also be worthwhile. Detailed understanding of the diverse material responses to optical excitation is expected to provide novel information, enabling the design of magnetic memories or ultrafast on-chip communication using spin waves.

Acknowledgment We thank Drs. C. Mitsumata, A. Yamaguchi, and T. Satoh for fruitful discussions and Mr. T. Yagi for the analysis of the magnetic domains. The experiments at the BL25SU beamline at SPring-8 were performed with the approval of the Japan Synchrotron Radiation Research Institute (JASRI) (Proposal Nos. 2011B1302, 2012A1232, 2012B1200, 2013A1482, 2013B1304, and 2014B1736). This work was partially supported by a Grant-in-Aid for Scientific Research (S, 18101004) and Grants-in-Aid for Young Scientists (B, 26790076 and A, 17H04920) from the Japan Society for the Promotion of Science, Projects for Innovative Quantum Functional Materials (PIQFUM), of the Ministry of Education Culture, Sports, Science and Technology (MEXT), and the Photon and Quantum Basic Research Coordinated Development Program of MEXT.

1) A. V. Kimel, A. Kirilyuk, P. A. Usachev, R. V. Pisarev, A. M. Balbashov, and Th. Rasing, Nature **435**, 655 (2005).
2) C. D. Stanciu, F. Hansteen, A. V. Kimel, A. Kirilyuk, A. Tsukamoto, A. Itoh, and Th. Rasing, Phys. Rev. Lett. **99**, 047601 (2007).
3) J. P. van der Ziel, P. S. Pershan, and L. D. Malmstrom, Phys. Rev. Lett. **15**, 190 (1965).
4) A. R. Khorsand, M. Savoini, A. Kirilyuk, A. V. Kimel, A. Tsukamoto, A. Itoh, and Th. Rasing, Phys. Rev. Lett. **108**, 127205 (2012).
5) K. Vahaplar, A. M. Kalashnikova, A. V. Kimel, D. Hinzke, U. Nowak, R. Chantrell, A. Tsukamoto, A. Itoh, A. Kirilyuk, and Th. Rasing, Phys. Rev. Lett. **103**, 117201 (2009).
6) C.-H. Lambert, S. Mangin, B. S. D. Ch. S. Varaprasad, Y. K. Takahashi, M. Hehn, M. Cinchetti, G. Malinowski, K. Hono, Y. Fainman, M. Aeschlimann, and E. E. Fullerton, Science **345**, 1337 (2014).
7) I. Radu, K. Vahaplar, C. Stamm, T. Kachel, N. Pontius, H. A. Dürr, T. A. Ostler, J. Barker, R. F. L. Evans, R. W. Chantrell, A. Tsukamoto, A. Itoh, A. Kirilyuk, Th. Rasing, and A. V. Kimel, Nature **472**, 205 (2011).
8) T. A. Ostler, J. Barker, R. F. L. Evans, R. W. Chantrell, U. Atxitia, O. Chubykalo-Fesenko, S. El Moussaoui, L. Le Guyader, E. Mengotti, L. J. Heyderman, F. Nolting, A. Tsukamoto, A. Itoh, D. Afanasiev, B. A. Ivanov, A. M. Kalashnikova, K. Vahaplar, J. Mentink, A. Kirilyuk, Th. Rasing, and A. V. Kimel, Nat. Commun. **3**, 666 (2012).
9) T. Satoh, Y. Terui, R. Moriya, B. A. Ivanov, K. Ando, E. Saitoh, T. Shimura, and K. Kuroda, Nat. Photonics **6**, 662 (2012).
10) Y. Au, M. Dvornik, T. Davison, E. Ahmad, P. S. Keatley, A. Vansteenkiste, B. Van Waeyenberge, and V. V. Kruglyak, Phys. Rev. Lett. **110**, 097201 (2013).
11) J. P. Park, P. Eames, D. M. Engebretson, J. Berezovsky, and P. A. Crowell, Phys. Rev. Lett. **89**, 277201 (2002).
12) S. Iihama, Y. Sasaki, A. Sugihara, A. Kamimaki, Y. Ando, and S. Mizukami, Phys. Rev. B **94**, 020401(R) (2016).
13) A. Kubo, K. Onda, H. Petek, Z. Sun, Y. S. Jung, and H. K. Kim, Nano Lett. **5**, 1123 (2005).
14) M. Battiato, K. Carva, and P. M. Oppeneer, Phys. Rev. Lett. **105**, 027203 (2010).
15) D. Rudolf, C. La-O-Vorakiat, M. Battiato, R. Adam, J. M. Shaw, E. Turgut, P. Maldonado, S. Mathias, P. Grychtol, H. T. Nembach, T. J. Silva, M. Aeschlimann, H. C. Kapteyn, M. M. Murnane, C. M. Schneider, and P. M. Oppeneer, Nat. Commun. **3**, 1037 (2012).
16) C. D. Stanciu, A. V. Kimel, F. Hansteen, A. Tsukamoto, A. Itoh, A. Kiriliyuk, and Th. Rasing, Phys. Rev. B **73**, 220402(R) (2006).
17) T. Ohkochi, H. Fujiwara, M. Kotsugi, A. Tsukamoto, K. Arai, S. Isogami, A. Sekiyama, J. Yamaguchi, K. Fukushima, R. Adam, C. M. Schneider, T. Nakamura, K. Kodama, M. Tsunoda, T. Kinoshita, and S. Suga, Jpn. J. Appl. Phys. **51**, 073001 (2012).
18) K. Vahaplar, A. M. Kalashnikova, A. V. Kimel, S. Gerlach, D. Hinzke, U. Nowak, R. Chantrell, A. Tsukamoto, A. Itoh, A. Kirilyuk, and Th. Rasing, Phys. Rev. B **85**, 104402 (2012).
19) N. Ogawa, W. Koshibae, A. J. Beekman, N. Nagaosa, M. Kubota, M. Kawasaki, and Y. Tokura, Proc. Natl. Acad. Sci. U.S.A. **112**, 8977 (2015).
20) M. Weiler, H. Huebl, F. S. Goerg, F. D. Czeschka, R. Gross, and S. T. B. Goennenwein, Phys. Rev. Lett. **108**, 176601 (2012).